IOP Publishing Phys. Biol. 17 (2020) 021001 https://doi.org/10.1088/1478-3975/ab694e

Physical Biology

OPEN ACCESS

TOPICAL REVIEW

Advanced fluorescence imaging of *in situ* protein aggregation

Meng Lu, Clemens F Kaminski and Gabriele S Kaminski Schierle[1]

Cambridge Infinitus Research Centre, Department of Chemical Engineering and Biotechnology, University of Cambridge, West Cambridge Site, Philippa Fawcett Drive, Cambridge CB3 0AS, United Kingdom

[1] Author to whom any correspondence should be addressed.

E-mail: gsk20@cam.ac.uk

RECEIVED
29 September 2019

REVISED
6 January 2020

ACCEPTED FOR PUBLICATION
8 January 2020

PUBLISHED
11 February 2020

Keywords: advanced imaging, protein aggregation, neurodegenerative diseases, super-resolution microscopy, structural progression

Abstract

The aggregation of intrinsically disordered proteins is a hallmark of neurodegenerative diseases, such as Alzheimer's, Parkinson's and Huntington's disease. Although we currently have a good molecular level understanding on how protein aggregation occurs *in vitro*, the details of its self-assembly in live cells are still mainly unknown. During the last ten years, we have witnessed the rapid development of advanced imaging techniques, especially super-resolution and fluorescence lifetime-based microscopy, in different areas of cell biology. These methods have been revolutionising our understanding of how proteins aggregate, providing unprecedented high spatial-temporal resolution which permits us to capture the kinetics of aggregate seeding and expansion, the motion and distribution of individual aggregates within the cells, and its structural change. In this article, we will review the study of *in situ* protein aggregation using advanced imaging techniques, with the focus on protein aggregate structure and its assembly dynamics.

Introduction

A key feature of biological systems is the ability to self-assemble its components. Complex biological organisms can be reduced to tissues, cells, organelles and ultimately—proteins. Protein folding and assembly are key in nearly all aspects of maintaining a functional biological system. In contrast, an imbalanced proteostasis is associated with a variety of diseases [1]. The failure of protein folding, and the subsequent events of protein aggregation and misallocation in cellular compartments is referred to misfolding disorders, including Alzheimer's (AD), Parkinson's (PD) and Huntington's disease (HD) (table 1), [2]. In the over 100 years of research on these misfolding disorders, since the discovery of AD by Dr Alois Alzheimer in 1906, we have learnt a great deal on disease development and the spread of its pathology throughout different brain areas of the patients. One of the key findings is the identification of amyloid fibrils and plaques that are formed by amyloid β ($A\beta$). Conventionally, the amyloid aggregation reactions are studied in the test tube. *In vitro* experiments have for example demonstrated how fibrillary aggregates elongate by the assembly of monomers of misfolded proteins at seeding sites [3, 4]. Such aggregate reactions take place in a highly controlled environment and display well-defined kinetics, thereby ignoring active processes and different compartments such as present in live cells. The understanding of the mechanistic process of aggregate formation and deposition in cells is of paramount importance in order to find therapeutic approaches to tackle these devastating diseases. To address this, it requires not only the observation at high resolution that can dissect the structure and morphology of aggregates but also direct observation of dynamic structural progression of protein aggregates in live samples.

In this review, we focus on advanced imaging methods (table 2) to study the structural progression of protein aggregates *in situ*. Fluorescence-lifetime imaging microscopy (FLIM) enables us to quantitatively detect the sensitive and fast changing state of amyloid aggregation in live samples. Next, super-resolution (SR) imaging, that breaks the optical diffraction limit, enables fast tracking of macromolecules in the native state, therefore demonstrating the dynamics of protein aggregates in real time. Following the outline of techniques, we discuss their application in the *in situ* investigation of amyloidogenesis, taking examples of studies performed in AD, PD and HD models.

FLIM

FLIM is an imaging technique based on the measurement of the exponential fluorescence decay

Table 1. Different characteristics of aggregates found in Alzheimer's, Parkinson's and Huntington's disease.

Disease	Protein	Characteristics of *in situ* protein aggregates	References
Alzheimer's disease	Amyloid-β ($A\beta$)	• Rapid protein assembly and aggregation • Defined fibril structures • Large filaments • Amyloid plaques formation	[22–37]
Parkinson's disease	α-synuclein AS)	• Slow aggregation process • Pre-fibrils are more toxic • Defined fibril structures • Lewy-body formation • Binding to synaptic vesicles	[38–46]
Huntington's disease	Huntingtin (Htt)	• Slow aggregation process • Formation of short fibrils • Formation of large aggregate structures, inclusion bodies (IBs) in cell centre • Aggregate expansion via diffusion and dynamic clustering	[47–58]

over time [5]. Conventional microscopy generates images by the contrast of fluorescence intensity, however, in FLIM the fluorescence lifetime of the fluorophore signal creates spatially resolved images. This permits the observation of contrast of different parts within the same sample, even if they are homogeneous in their fluorescence intensity, thus providing another dimension to visualise the properties of the labelled samples. FLIM is compatible with other imaging techniques. It can be applied in confocal microscopy, two-photon excitation microscopy, and multiphoton tomography mode. Amyloidogenesis is accompanied by a change of intrinsic energy states which is be reflected in fluorescence lifetime [6]. Therefore, FLIM provides a particularly sensitive readout of the aggregation state, which is robustly quantifiable for experiments performed *in vitro* and *in vivo* [7].

Super-resolution microscopy

Due to the nature of light diffraction, the resolution in optical microscopy is proportional to the light wavelength, and to the numerical aperture of the illumination source, described by Ernst Karl Abbe in 1873 and further discussed by Rayleigh and others. However, the ongoing need to image biological structures and processes existing below this resolution limit has triggered the development of super-resolution microscopy that bypasses the diffraction limit of optical systems and brings optical microscopy into the nanodimension. A variety of techniques have been invented to achieve spatial resolution below the diffraction limit. Here, we will focus on the approaches that have been commonly used in the study of protein aggregation, which include structural illumination microscopy (SIM), stimulated emission depletion (STED) and stochastic optical reconstruction microscopy (STORM)/photo-activated localisation microscopy (PALM).

SIM

SIM is a wide-field fluorescence imaging technique, which doubles the resolution of images when compared with standard confocal microscopy [8]. The fluorescence excitation light is scrambled to generate a patterned illumination, usually stripes, before it is projected onto the samples. The pattern position and orientation are shifted a number of times and the fluorescence emission is recorded for each of these positions and orientations. The patterned illumination produces Moiré fringes as an interaction between the patterned illumination and the sample. In Fourier space, the Moiré fringes contain additional high spatial frequency information from the sample. With sufficient shifts of the excitation pattern, this high frequency information that conveys the fine structural details of the sample can be extracted by algorithms producing reconstructed images with a lateral resolution approximately twice of the diffraction-limited settings.

There are several advantages that make SIM suitable to study the structural progression and dynamics of intracellular aggregates *in situ*. First, SIM does not require specialised fluorophores and is thus compatible with other fluorescence microscopy techniques. Thus, SIM enables a higher resolution than can be achieved with wide-field or confocal microscopy but with the use of the same sample preparation procedure. Second, the spatially structured illumination light can be applied to three dimensions and doubles the axial and lateral resolution. Third, as a wide-field based imaging technique, SIM is faster in its image acquisition than localisation microscopy, such as STED and STORM/PALM, although it has a lower

Table 2. Different characteristics of the advanced fluorescence microscopy methods in the study of *in situ* protein aggregates.

Microscopy method(s)	Technique principles	Spatial resolution	Temporal resolution	Labelling dyes
Fluorescence-lifetime imaging microscopy (FLIM)	Fluorescence lifetime reflects on the intrinsic energy state of amyloid aggregates.	200–250 nm	Minutes scale (dependent on settings)	YFP [6], HiLyte Fluors [27], mCherry [34], EGFP [49], RFP [49]
Structural illumination microscopy (SIM)	Patterned illumination of samples permits the extraction of high frequency information, therefore of fine structural details.	80–100 nm	Fast image acquisition (at the same scale of widefield microscopy)	Compatible with most fluorophores, no need for special labelling: mCherry [34], SNAP [54], EGFP [57], Janelia Fluors [58]
Stimulated emission depletion (STED)	Depletion of the peripheral emission of fluorophores narrows the PSF during image acquisition.	40–50 nm	Same as confocal microscopy	ATTO [35], Alexa [42, 46], Abberior [42], STAR Fluors [45]
Localisation microscopy (STORM, PALM)	Stochastic activation of well separated individual fluorophores produces a single-molecule image of each fluorophore.	20 nm	Slow image acquisition, minutes scale dependent on settings	Photoswitchable fluorophores: HiLyte Fluors [27], Alexa Fluors [37, 43, 44, 58], eYFP [51], Cy3[55], Halo-tags [58], Janelia Fluors [58]

spatial resolution compared to the latter. This feature greatly enhances its application in live cell imaging. The recent development of a SIM reconstruction algorithm based on Hessian matrixes can achieve 188 Hz at 88 nm spatial resolution [4], which permits the observation of the fast dynamics of mitochondrial cristae and the enlarged fusion pores during vesicle exocytosis which have not been observed previously.

The main disadvantage of SIM is its only moderate resolution improvement compared to localisation microscopy. Its complex setup can further introduce errors, such as grating misposition or refractive index mismatch. Furthermore, the misuse of post-acquisition processing algorithms can also lead to artefacts in the reconstructed images.

STED

STED is based on scanning microscopy, where sub-diffraction limited resolution is achieved by the selective deactivation of fluorophores around the scanned diffraction-limited excitation spot [9]. This is achieved by pairing two synchronised laser pulses. Fluorophores are excited by the first laser pulse which generates an ordinary diffraction limited focus. This is immediately followed by a second doughnut-shaped laser which is red-shifted in frequency to the emission wavelength of the dye so as to deplete the emission around the excited focus. Therefore, only the fluorescence from molecules in the centre of the doughnut—where the second laser intensity is zero—is measured by single-photon sensitive detectors.

Since STED bypasses the diffraction limit by narrowing the point spread function (PSF) during image acquisition, it does not require subsequent image reconstruction and generates instant super-resolution imaging. Therefore, it can avoid potential artefacts caused by misuse of the reconstruction algorithms. The STED design, theoretically, enables the resolution of STED microscopy to reach the molecule's size. However, the practical resolution is limited by the signal-to-noise ratio (SNR), which can be affected by multiple components of the instrument setup, such as the efficiency of the single photon detector, the focal intensity distribution of the beams, the precise alignment of the two laser beam foci, and fluorophore's photostability and brightness. Currently, the lateral resolution of STED under experimental conditions is 20 nm and the axial resolution around 40 to 50 nm.

STED requires strong laser illumination to deplete the peripheral emission, and higher resolution requires higher intensity of the laser power. This will lead to greater photobleaching of the fluorophores and phototoxicity of the samples compared to SIM. Therefore, it is still a challenge to perform long-term imaging in live samples. Furthermore, many fluorophores suitable for STED microscopy are not membrane permeable, limiting its application in recording the dynamics and structural progression of aggregates and organelles during live cell imaging. In terms of imaging speed, STED microscopy stimulates fluorophores between the ON and OFF states 'instantaneously', therefore, it can achieve the same temporal resolution as confocal microscopy. However, in scanning microscopy, the increase of spatial resolution is followed by the decrease of pixel size, which leads to a smaller field of view. Therefore, for the same fluorescence intensity, one has to sacrifice the spatial resolution or the field of view to gain extra temporal resolution. This also limits its application to image structural protein aggregate progression inside cells.

STORM/PALM

STORM and PALM are wide-field based imaging methods that permit images with a spatial resolution greater than 20 nm to be obtained [10, 11]. The STORM method relies on the stochastic activation of individual fluorophores with photoswitchable properties. During image acquisition, single fluorophores 'blink' by a process of random activation, going from an 'OFF' state to an 'ON' state, which is then quickly deactivated by photobleaching. For successful STORM imaging, the stochastically activated fluorophores must be well isolated from each other at any time to exceed the diffraction limit that is greater than approximately 250 nm. The stochastic activation of sparse fluorophores can then produce a single-molecule image of each fluorophore that does not overlap. Repeating this process many times will gradually image most fluorophores, thus mapping the samples in a single molecule imaging method. Thousands of single wide-filed images are collected during STORM acquisition. Since individual molecules are well separated, the fluorophores can be precisely localised in each activation event by fitting the resulting point spread function to a 2D Gaussian function. Therefore, overlapping all the measured positions of fluorophores will then produce the final super-resolution image.

Distinct from the patterned illumination of SIM and stimulated depletion of STED, STORM and PALM use multiple (typical thousands of) cycles of activation, excitation and de-activation/bleaching of photoswitchable fluorophores, which significantly extend the acquisition period. This therefore limits their application to mainly fixed samples. Furthermore, the extended high power laser illumination causes strong photobleaching and phototoxicity in the samples.

A number of studies have been published to apply PALM/STORM for live cell imaging, however, it is still a challenge to perform long-term imaging of live samples. Based on the current STORM/PALM setup, the ability to perform long-term imaging ultimately depends on whether enough photons can be collected in a short time. A significant increase of the fluorophore brightness in its 'ON' state can generate enough photons to be detected, so that the number of repetitive imaging cycles can be greatly reduced, and thereby decrease phototoxicity.

High-density localisation microscopy

Localisation microscopy methods rely on repeated imaging acquisition of well-separated fluorophores. Consequently, the temporal resolution of localisation microscopy is low and not applicable to live and dynamic samples. To overcome this, a number of imaging methods based on high-density localisation microscopy have been developed to enable faster acquisition and thus live-cell imaging. These methods rely on the stochastic fluctuations of the fluorophores and permit fluorophores to overlap, and therefore avoid the synchronized photoactivation. Imaging methods based on the above principles are; compressed sensing [12], bleaching/blinking-assisted localisation microscopy (BaLM) [13], super-resolution optical fluctuation imaging (SOFI) [14] and super-resolution radial fluctuations (SRRF) [15], and new analysis approaches, such as multi-emitter fitting [16, 17], artefact-free high-density localisation microscopy analysis [18], and Bayesian analysis of bleaching and blinking (3B) [19] to name a few. All these methods pave the way for imaging of *in situ* protein aggregates and their associated cellular structures in live cells and thus in a dynamic manner.

Application of advanced fluorescence microscopy in the study of *in situ* protein aggregation

Amyloid β aggregation

The formation of amyloid aggregates is a hallmark of AD. Amyloid precursor protein (APP) is cleaved by γ and β-secretase, producing $A\beta$ peptides that are most commonly 40 or 42 residues in length [20]. These $A\beta$ peptides can be released into the extracellular environment to form plaques that are coupled to synapses and lead to synaptic disfunction and loss [21]. On the other hand, $A\beta$ peptide has also been found in intracellular organelles, such as multivesicular bodies [22], Golgi [23], endosomes [24] and mitochondria [25]. The abundant $A\beta$ peptide in intracellular membrane systems thus provides a substantial source for the production of intracellular aggregates, which display multiple configurations and states that are associated with different physiological or pathological effects [26]. In addition, extracellular $A\beta$ peptides taken up into the cell via endocytosis also leads to rapid intracellular aggregation [27].

The aggregation of $A\beta$ peptides has been the subject of extensive studies for decades [28]. Most of these studies are performed applying an *in vitro* approach for which protein concentration, diffusion and aggregation kinetics are well controlled. *In vitro* studies have provided detailed insight into mechanisms of protein aggregation and enabled building precise mathematical models to describe and simulate the phenomenon of protein aggregation [29], however, data gained from test tubes are often not representative on mechanisms taking place in the cell, where the molecular environment is fundamentally different [30]. First, proteins inside the cell are normally heterogeneously distributed and can concentrate in a specific subcellular context, which is a challenge to be simplified in homogeneous solutions. Secondly, frequent and dynamic interaction among intracellular molecules and compartments significantly increase the complexity of the self-assembly reactions of $A\beta$ peptides, however, this is largely neglected in *in vitro* experiments. Last, active transport, phase transition, and compartmentalisation, only featured in an intracellular environment, will also strongly affect the kinetics and attributes of protein aggregation [31].

To gain the mechanistic insight of $A\beta$ aggregation in a disease relevant state, there is thus a great demand for refined methods that can directly examine the self-assembly reactions of $A\beta$ (and other aggregation-prone proteins) non-invasively in cells. Advanced optical microscopy, including FLIM and methods of super-resolution imaging as introduced above, are particularly suited for this task, providing fast tracking of aggregation states, dynamic motions and highly-resolved structures of *in situ* aggregates.

Using FLIM, Esbjörner and colleagues [27] imaged the aggregate formation of $A\beta$ (1–40) and $A\beta$ (1–42) in live cells. Endocytic uptake of both peptides resulted in their localisation in lysosomes, where their accumulation led to aggregation. In the early stage of endocytosis, and despite the intensity images showed the accumulation of $A\beta$ peptides inside the cell displayed an increased brightness when compared with the peptides in the culture medium, the lifetime images taken by FLIM showed no significant difference, indicating the similar structural state of $A\beta$ peptides in both conditions. However, longer incubation of peptides with cells, which led to sufficient internalisation of the peptides into lysosomes, resulted in a prominent drop of fluorescence intensity, reflecting the aggregation state of $A\beta$ peptides. However, the fluorescence intensity of the peptides was kept at a similar level with those in the early stage of endocytosis. Therefore, FLIM clearly distinguishes the different states of aggregation-prone proteins and is thus independent of the fluorescence intensity, providing a fast and non-invasive measurement of protein aggregation in live cells. Later in this study, the authors also applied direct stochastic optical reconstruction microscopy (*d*STORM) to analyse the physical appearance of the intracellular aggregates showing reduced fluorescence lifetime. Aggregates formed by $A\beta$ (1–40) displayed different morphology to $A\beta$ (1–42), as $A\beta$ (1–40) aggregates were mainly spherical and approximately 160 nm in diameter whereas $A\beta$ (1–42) aggregates include both spherical and elongated species with an average size of 225 nm. Therefore, *d*STORM successfully reveals the structural difference between the two main $A\beta$ peptides which are within 100 nm and hard to be resolved by other optical methods.

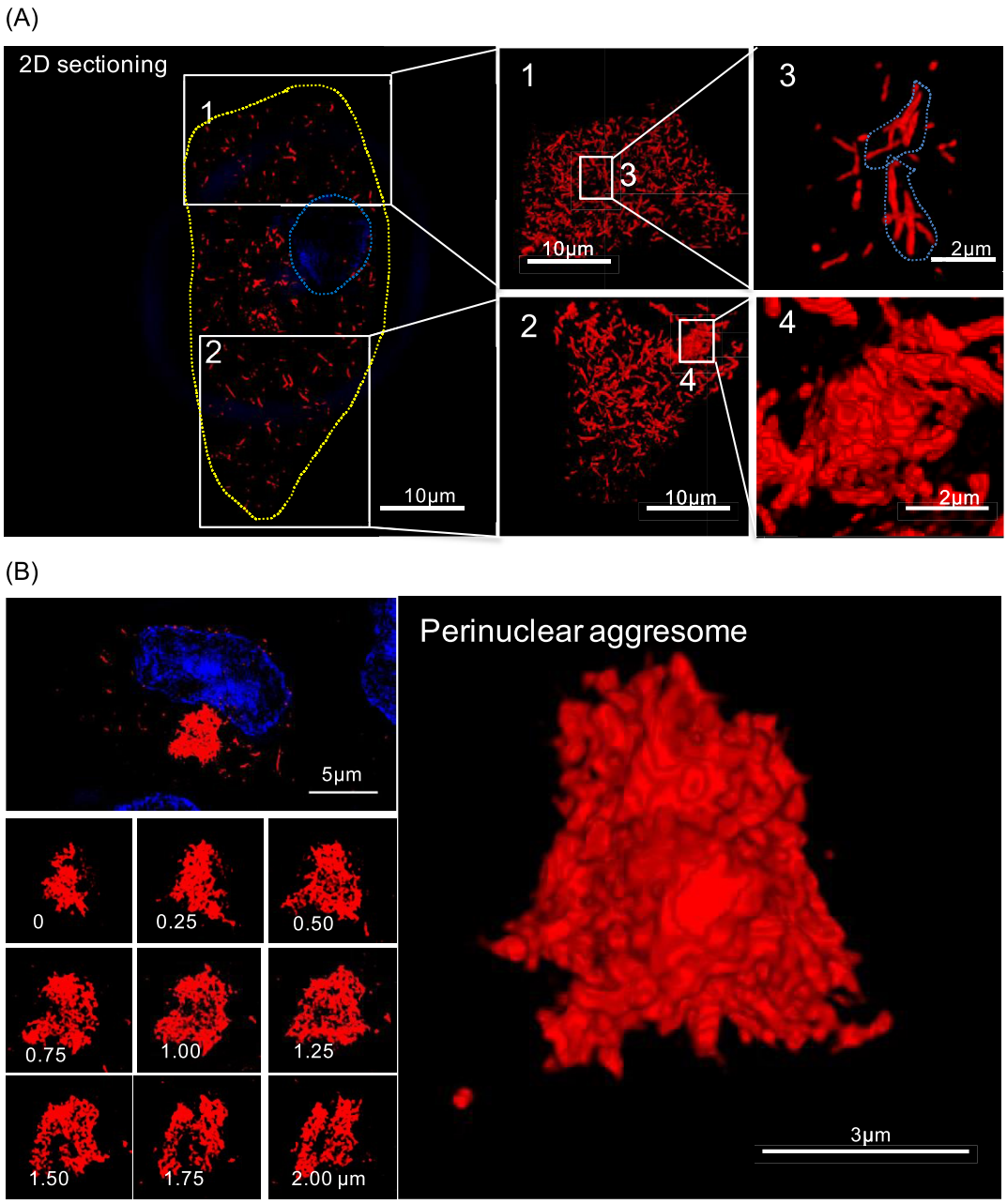

Figure 1. Super-resolved structures of intracellular Arctic mutant aggregates. This research was originally published in the Journal of Biological Chemistry, with permission from [34]. (A) Left: a section slice showing an Arctic mutant-expressing cell containing numerous fibrillary fragments, which are in different states of aggregation in the cytosol. Nucleus stained with Hoechst 33 342 (blue; and outlined with a blue dashed line). Yellow dashed line shows the outline of the cell. The zoomed regions are numbered. Middle and right panels are the projected views from 3D rendering. Image 3 shows oligomers (yellow arrows), single fibrils (green arrows) and fibril bundles (blue arrows). Image 4 shows a fibril cluster. (B) High resolution SIM images of an aggresome. Nucleus stained with Hoechst 33 342 (blue). Left panel: *z*-stack sectioning slice of an aggresome that contains tightly connected fibrillary fragments. Right panel: projected view from 3D rendering of the images from the left panel.

Several mutations of Aβ42 have been identified in genetic studies of AD. Among these, the Arctic mutation (APP E693G; Aβ42 E22G) [32] is the most aggressive in terms of aggregation and leads to an early accumulation of intracellular Aβ42 aggregates [33]. However, little information is known about its intracellular amyloidogenesis, such as how the Aβ42 E22G mutant rapidly assembles to form aggregates and whether these aggregates feature homogeneous structures or not in live cell models. To address these questions, we carried out direct, in-cell measurements of Aβ42 aggregation kinetics using FLIM and SIM [34]. The fluorescence lifetime decreased to different degrees in the same cells, indicating that the aggregates formed by the Arctic mutant are heterogeneous in structures. This was further confirmed by the fine structural information revealed by SIM. Following induction of the Arctic mutant expression, five states of intracellular aggregate—oligomers, single fibrils, fibril bundles, clusters and aggresomes rapidly

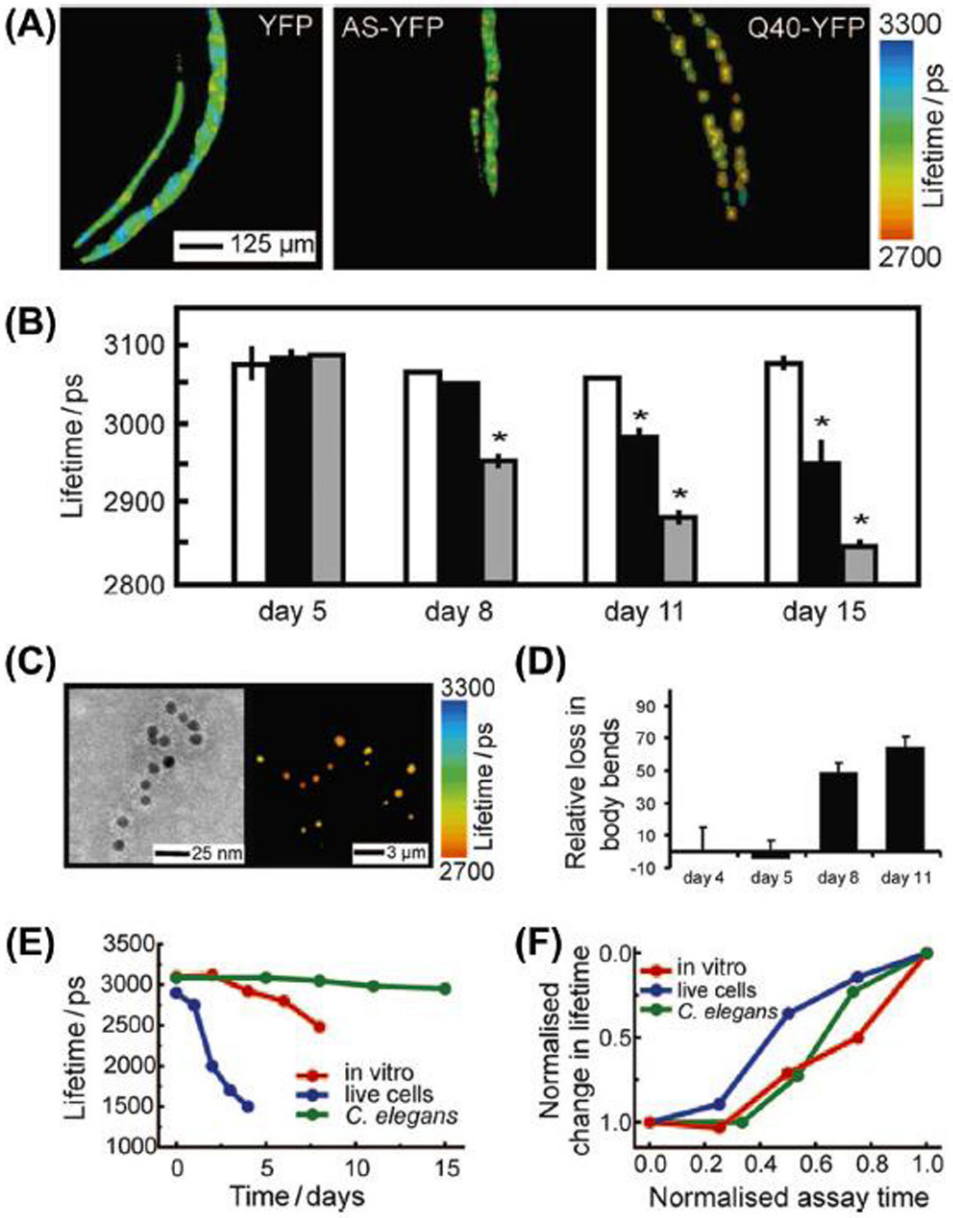

Figure 2. TCSPC lifetime imaging distinguishes the nature and kinetics of the aggregation of amyloidogenic YFP fusion protein variants during ageing in a living animal. Copyright Wiley-VCH Verlag GmbH & Co. KGaA. Reproduced with permission from [6]. (A) Left: TCSPC image of YFP transgenic *C. elegans* at day 11; middle: TCSPC image of AS–YFP transgenic *C. elegans* at day 11; right: TCSPC image of Q40-YFP transgenic *C. elegans* at day 11. Note how the fluorescent aggregates display a strong reduction in the fluorescence lifetime (red colour) with time. (B) Mean fluorescence lifetimes of the whole anterior part of transgenic worms expressing YFP (white), AS–YFP (black), and Q40-YFP (grey) during ageing of the animals, determined at various days during the assay (mean lifetime SEM, ANOVA with Scheffes' post hoc test, $p < 0.05$). (C) *Ex situ* studies of *in vivo* aggregated AS–YFP. Left: anti-AS immunogold-labelled TEM image of cell extracts from aged AS–YFP transgenic *C. elegans* (day 15). Only pre-fibrillar aggregates of AS–YFP are observed in these samples. Right: TCSPC image corresponding to the same sample as that shown on the right. (D) AS–YFP-dependent toxicity during ageing in *C. elegans*. The plot shows the ratio (%) of number of bends per minute for the AS–YFP transgene versus the YFP only transgene. Because of the selective expression of the transgene in muscle cells, the toxicity phenotype is a perturbation of the motility of the worm and the toxicity readout is a reduction in the number of bends per minute. (E) Time-dependence of the decrease of fluorescence lifetime for AS–YFP in the three systems studied herein (*in vitro*, red; living SH-SY5Y cells, blue; living *C. elegans*, green). (F) Normalised kinetics of AS–YFP aggregation *in vitro* and *in vivo* determined by the decrease in fluorescence lifetime. The colour code is the same as in (E).

developed. In the later state of amyloid development, different categories of aggregates coexist in the same cells, generating a highly complex mixture of aggregates, shown in figure 1. The application of 3D SIM not only allowed us to visualise the single fibrils formed in the initial stage but also to resolve the highly compact inner-structures of aggresomes that are assembled by numerous fibrils and clusters. This study performed under in *in situ* conditions thus uncovered the basis of structural progression of Aβ42, highlighting the heterogeneity of Aβ42 aggregates even in the same cellular environment and the different developmental stages in aggregate formation. Therefore, effective clearance of intracellular aggregates may require the specific design

of compounds that can target the corresponding state, as compounds inhibiting oligomer formation may not be effective in breaking aggregate clusters down.

Apart from the studies of aggregate morphology and structures, super-resolution imaging is also suited to investigate the subcellular localisation and interaction with organelles, which is of significance to understand the disease mechanism in AD. Using STED microscopy, Yu and colleagues [35] demonstrated that neuronal Aβ42 is enriched in small vesicles at the presynapse rather than at postsynapse of hippocampal neurons. The presynaptic vesicles that contain Aβ42 clusters connected to stubby spines and mushroom spines, indicating the broad association of Aβ42 with different neuronal structures. Another study performed by measuring the fluorescence life change of BODIPY-tagged Aβ42 showed their interaction with cellular plasma membrane, which was supported by the observation of membrane disruption and cell damage [36].

Imaging in thick tissues is a challenge for super-resolution imaging because of the strong background noise. However, the recent development of super-resolution imaging methods has shown their potential to dissect the organisation of aggregates in brain tissues. Mlodzianoski and colleagues combined active shaping of PSFs and efficient adaptive optics to construct robust single-molecule switching microscopy imaging for imaging in tissue [37]. This enables the imaging through 30 μm-thick brain sections to visualise the structure of $A\beta$ filaments in an AD mouse model at the nanoscale. The reconstructed volumetric view of amyloid plaques displayed a spectrum of different sizes from 5 μm, with a loose organisation of filaments, to larger than 15 μm, with a strong compaction of fibrils. The filaments below the diffraction limit that are not possible to be identified individually by conventional microscopy, can now be distinctly observed and reconstructed in the plaque centre in thick tissue by 3D-SMSN.

α-synuclein aggregation

Following AD, Parkinson's disease (PD) is the second most common neurodegenerative disease. PD is characterised by the formation of Lewy bodies (LBs) and loss of dopaminergic neurons [38]. A variety of molecules have been identified in LBs, in which α-synuclein (AS) is the primary structural component [39]. The proliferation of AS aggregates is strongly linked to the disease propagation, however, the mechanism of self-assembly of AS under physiological condition remains elusive. AS is a 140-residue protein and considered to be an intrinsically disordered protein.

Both wild type and disease-related mutants of AS form amyloid-like fibrils upon prolonged incubation in solution [40], which is believed to form the basis of LBs in PD. AS assembles into a variety of intermediate structures in the process of fibril formation, which are termed protofibrils [41]. Soluble oligomers of AS display either spherical, ring, or string like features as shown by electron microscopy, and gradually assemble into insoluble fibrils. However, neither protofibrils nor fibrils have been properly examined in cells. Using STED microscopy, Moors and colleagues studied the distribution of the post-translational modifications of AS in neurons, for example phosphorylation of AS at Serine 129 (Ser129-p AS), which is implicated in PD pathology. The STED imaging resolved a systematic onion-like architecture of LBs. The Ser129-p AS accumulated at the periphery of these onion-skin type LBs and were associated with a cage-like framework of intermediate neurofilaments [42].

As AS assembles into different forms of aggregated species, which of them are toxic to neurons is still under debate. In the following study, Pinotsi and colleagues applied *d*STORM to monitor the fate of different forms of AS in neurons and examined the cellular response of the formation of AS aggregates [43]. First, they showed that exogenous fibrils added to neurons act as seeding sites for fibril elongation reactions and consume endogenous AS and suppress its *de novo* aggregation, which is protective to neurons. In contrast, monomeric AS added to neurons nucleates with endogenous AS to form intracellular aggregates and triggered apoptosis. Treatment of external monomeric AS led to neuron death, however, this can be rescued by pre-treatment of neurons with preformed fibrils. This study thus suggests a neuroprotective role of fibrillary species compared with monomeric AS. *d*STORM here allows direct and non-invasive observation of self-assembly processes at the nanoscale in the cell, correlating the seeding mechanisms of AS with its neuronal toxicity in neurons.

This is further supported by a study performed in the nematode worm *Caenorhabditis elegans* (*C. elegans*). The model organism was engineered to express AS-YFP for measurement of protein aggregation by FLIM [6]. This permits the kinetic imaging of AS aggregation in a multicellular living organism, thus offers clues to its associated effects in different parts of the body, as shown in figure 2. In addition to a simple observation of aggregate presence, this method directly reveals the states of aggregation, from monomers, oligomers and fibrils. During 15 d of AS-YFP expression and tracking, the worms displayed a strong phenotype (loss of body bends) due to cellular damage when compared with control animals expressing YFP only, which correlates with the observed decrease in the fluorescence lifetime of AS-YFP. The aggregate species from *C. elegans* were further extracted at different time points for parallel time-correlated single photon counting (TCSPC) and immune-TEM analysis, which validates that these aggregates are pre-fibrillar species, indicating the formation of less ordered fragments rather than more matured amyloid fibrils. Therefore, similar to the above study, the latter study provides

evidence that pre-fibrillar rather than fibrils are the most toxic species in AS associated disorders.

The intracellular AS aggregation induced by exogenous fibrils has also been used to study the structures of aggregates in mouse hippocampal primary neurons [44]. A newly developed technique that combines multiple-plane phase retrieval and super-resolution optical fluctuation imaging permits the visualisation of the 3D architecture of newly formed AS aggregates. Using correlative light and electron microscopy, Shahmoradian and colleagues found a crowded environment of membrane mixtures in the LBs from human brain tissue [45].

In addition to the study of the structural progression of AS associated aggregates, super-resolution imaging has also demonstrated an ability to examine the AS interaction with small vesicles in cells. To study how AS modulates the vesicle homeostasis at the presynaptic terminal, Lautenschläger and colleagues applied STED microscopy and showed that synaptic vesicles are surrounded and glued together by AS. Furthermore, *d*STORM images of synaptosomes revealed that calcium mediates the localisation of AS at the pre-synaptic terminal, and that an imbalance in calcium or AS can cause synaptic vesicle clustering [46]. Therefore, both AS and calcium levels need to be finely balanced to prevent neuronal toxicity. Advanced imaging methods applied in this study enables the measurement of molecular interaction and thus elucidates the binding mechanism of AS and synaptic vesicles, which provides new insights in understanding synucleinopathies.

Polyglutamine aggregation

PolyQ diseases are a group of neurodegenerative disorders caused by the expansion of repeat glutamine codons in various unrelated protein-coding genes. These genetic disorders caused by polyQ include HD, spinocerebellar ataxia and bulbar muscular atrophy [47]. Accumulation of misfolded polyQ leads to the formation of aggregates in both the cytosol and nucleus [48].

Intracellular polyQ aggregates appear to be structurally heterogeneous [49], being composed of a mixture of oligomers, fibrils and inclusion bodies (IBs) [50]. However, the structural identities of toxic aggregate fragments in polyQ associated pathogenesis remain ambiguous. Sahl and colleagues first used single-molecule-based super-resolution imaging to study the spatial distributions of fluorescently-labelled Htt-exon1 species in the cell model PC12m [51]. Apart from the large inclusion bodies depositing at the cell centre, they also observed fibrillar aggregates of pathogenic polyQ tracts ~100 nm in diameter and up to ~1–2 μm in length after targeted photo-bleaching of the inclusion bodies. This revealed that the intracellular fibrils feature a distinct length cut-off at ~1.5 μm and undergo subsequent coalescence (bundling/piling). Imaging the aggregate structures at different time points also revealed the sequential events of protein aggregation in cells: fibrils arise abundantly across the cytosol only after a prominent IB was generated. IB formation has been argued to sequestrate the smaller forms of aggregates after the degradation system has been compromised [52]. The multitudinous emergence of polyQ fibrils may indicate that the IBs have been saturated after over-loading with misfolded proteins. This study demonstrated the ability of super-resolution microscopy at detecting and measuring the structures of intracellular polyQ fibrils. To investigate the structural progression of intracellular aggregates from fibrils to aggresomes that is the microtubule dependent IB [53], we constructed a set of cell lines that can express SNAP tag labelled partial Htt exon1 at low, intermediate and strong expression levels [54]. Aggregates formed at different expression levels and time points were imaged by SIM. We found that aggresomes in cells with weak or intermediate-expression levels are both smaller and less compact than in cells with strong expression levels. Irrespectively, all aggresomes are composed of short fibrils and small clusters as revealed by 3D SIM. At high expression levels, we also identified long fibrous structures of SNAP-HDQ72 surrounding the nuclear envelope which are not observed in cell lines with weak or intermediate-strength promoters. Although the large aggresomes in cell models are regarded as fibril-sequestering protective entities [54], the long-term deposition of aggresomes in the perinuclear area in this study is associated with abnormal nuclear morphology [54]. A following-up study examined the molecular consequences of the aggresome deposition and revealed that aggresomes blocked the formation of mitotic spindles and led to mitotic defects and accumulation of DNA double-strand breaks [48].

The mechanistic process of protein aggregation is clearly of pathological significance, for example, how the motion patterns of small aggregates interact with large molecules or organelles in the cell. Conventionally, the studies on mechanistic processes of misfolded protein assembly are performed in the test tube. *In vitro* experiments have well characterised the growth of huntingtin exon 1 aggregates via adding monomers at seeding sites [55]. However, how the fibrils formed in this well-adjusted solution interact with cellular structures was not known. The pathological effects of polyQ fibrils have been confirmed by a recent study on the structures of polyQ fibrils by correlative microscopy of cryo-electron tomography and optical microscopy, showing that the fibrils in the inclusion body deform ER membranes and alter ER organisation [56].

In addition to resolving the fine details of aggregate structures, fast-SIM is well suited to monitor the dynamics of aggregates in cellular environments. A recent study from us tracked the entire fate of aggregates, from single fibril to large aggresome, in the cytosol [57]. Fast-SIM applied in this study permitted

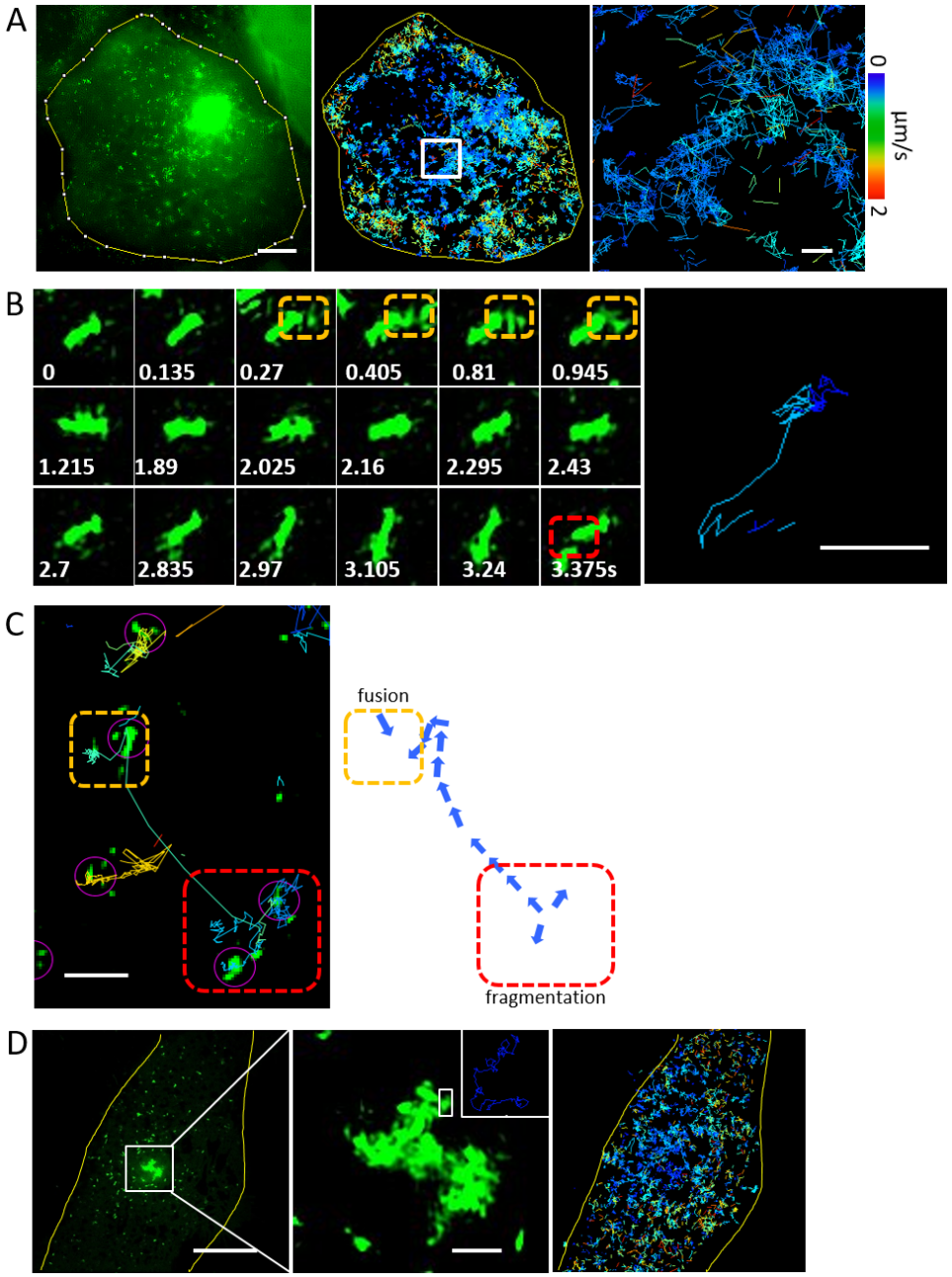

Figure 3. PolyQ aggregates undergo frequent fusion and fragmentation events in the cell. This research was originally published in the Journal of Biological Chemistry, with permission from [57]. (A) High-speed SIM recordings of intracellular aggregate dynamics. All small aggregates are subjected to dramatic random movements, which lead to collisions and contacts among clusters. Using an SPT algorithm, we identified individual particles and analyzed their trajectories in time at a frame rate of 5 Hz (middle panel). The right-hand panel shows a zoomed-in version of the region in the white rectangle. The velocity spectrum shown applies to all panels. Scale bars, 5 μm (left panel) and 1 μm (right panel). (B) Example images of individual particles in quasirandom motion (6 Hz). The image on the right demonstrates the aggregate trajectories. Numbers in white show the time (in seconds) of each frame. Dashed orange and red rectangles highlight fusion and fragmentation events, respectively. Scale bars, 500 nm. (C) Aggregate motion includes both active and passive transport components. The purple arrows highlight regions where small clusters where identified in the automated analysis. The dashed orange and red rectangles indicate regions where fusion and fragmentation take place, respectively. Scale bar, 2 μm. (D) A cell containing an aggresome in the center and small aggregates in cytosol (left panel). A zoomed-in region shows that the loose clusters in the periphery of the aggresome are highly mobile (middle panel). The inset in the top right of the middle panel shows motion paths of individual fragments within the aggresome, which are highlighted in the white square. SPT reveals that the mobility of aggregate fragments is higher in the cytosol than in the aggresome (right panel). Scale bars, 5 μm (left panel) and 1 μm (middle panel).

us to trace the nucleation and expansion phases of aggresomes in the perinuclear region. This uncovered that passive transport played a significant role in the formation of aggresomes, which was believed to be mainly driven by active transport. Consequently, image acquisition by fast-SIM was followed by single particle tracking (SPT), and mathematical modelling of aggregate transport in the cell. We established two phases of aggresome formation. First, active transport of small aggregates leads to the seeding sites of aggresome, which determines the position of aggresomes. Second, diffusion drives protein aggregates, which are overwhelming in the cytosol, to assemble at the seeding site formed in the first stage

which consequently rapidly expands the aggresome. The nascent aggresome in the perinuclear area grows in size with increasing surface area, thus accelerating the capture rate for aggregate species diffusing in cytosol. Therefore, in the second phase, aggregate assembly via diffusion gradually becomes the primary route for aggresome growth and the contribution of active transport is negligible. This high spatial-temporal imaging of *in situ* aggregates demonstrates that the assembly of short fibrils into larger structures, such as aggresomes, is primarily driven by passive transport rather than the reaction of end-on monomer addition to fibrils as shown in the test tube. The SPT also showed that fast fusion and fragmentation events of aggregates take place frequently in the dynamic cellular context (figure 3), which may explain the formation of short fibrils and branched clusters of ca. 500–1000 nm in diameter rather than long linear fibrils.

In another study of aggregate dynamics in cells, Li and colleagues used single-molecule localisation microscopy to classify three distinct dynamic states of mHtt in living cells—(1) fast diffusion, (2) dynamic clustering and (3) stable aggregation [58]. This shows how mHtt forms aggregates and dynamically disrupts the gene control mechanisms in neuronal cells. mHtt aggregates inside the nucleus can form 'sticky' decoy traps that impede target search processes of key regulators involved in neurological disorders.

Conclusions and future outlook

Advanced optical microscopy has opened new avenues for direct observation and measurement of large molecules in live samples. Here, we have reviewed the application of FLIM and super-resolution imaging in the study of *in situ* protein aggregation. By detecting fluorescence lifetime of fluorophore using FLIM, it is possible to gain kinetic information on the aggregation state in both cell models and in living organisms such as *C. elegans*. Single molecule detection based STORM and PALM obtain images of aggregate structures at a resolution approaching that of electron microscopy, but retain the advantages of optical techniques for application in cells and organisms. Wide-field based SIM doubles the resolution of conventional light microscopy and achieves fast image acquisition rate, which is of great significance to visualise the intracellular dynamics of aggregates and organelles. All these advanced optical imaging methods have revolutionised our studies to visualise aggregate structures and dynamics *in situ*. Here, we review the implementation of advanced fluorescence microscopy in the studies of protein aggregates in AD, PD and HD. Beyond the proteins summarised here, these imaging methods have been applied to characterise a variety of other protein aggregates that are associated with ageing and neurodegeneration. Combining electron microscopy and SIM, Zhou and colleagues found that ER-associated aggregation sites of misfolded proteins are frequently bound or captured by mitochondria that further control the dynamics and asymmetric segregation of aggregates in dividing yeast cells [59]. Another study used a combination of transmission electron microscopy, FLIM and SIM to characterise the structures of ageing dependent protein aggregates in *C. elegans*, which contributed to functional decline in *C. elegans* [60].

The combination of these techniques provides a global and direct observation of multiple structures and events, from single fibrils to large inclusion bodies, in their native environment at high spatial-temporal resolution and in a quantitative way. Despite these advances, there is room for further improvement. Long-term imaging of aggregate formation, from oligomers to large inclusions, is still a challenge for super-resolution imaging. First, phototoxicity during long-term imaging will lead to irreversible damage of the cellular structures, especially the membranous organelles. This will cause biased interpretation in the study of aggregate associated cellular damage. Second, photobleaching of the fluorescence markers decreases the SNR of raw images and thus makes it hard to generate reconstruction. Last but not the least, since aggregated species are highly heterogeneous, the compact structures such as inclusion bodies display ultra-strong signals while their peripheral species such as single fibrils and oligomers demonstrate much weaker signals. Therefore, it is still a challenge to capture multiple structures in the same imaging field. Overall, imaging with faster speed and higher resolution, longer imaging time with less phototoxicity and photobleaching will lead us to record more details of the aggregate structural progression in *in situ* experiments. To achieve this, we need to coordinate the development of all the related subjects, from the chemical synthesis of fluorescent dyes of high stability and brightness, to the manufacturing of cameras with higher sensitivity etc.

More recently, deep learning, as a state-of-the-art method, has been actively introduced in the field of optical imaging. Artificial neural network based deep learning can significantly facilitate the imaging processing, including denoising of the degraded images [61], segmentation of different objects [62], improving reconstruction [63] and sample classification [64]. With continued advances in instrument design, fluorophores and post-acquisition processing, the use of advanced microscopy will provide a more complete understanding of the mechanisms of *in situ* protein aggregation and their pathological effects.

Acknowledgments

We thank Dr Edward Ward for helpful discussions and for his comments. We acknowledge funding from Infinitus (China) Company Ltd, Wellcome Trust, UK Medical Research Council (MRC), and Alzheimer's Research UK (ARUK).

ORCID iDs

Meng Lu https://orcid.org/0000-0001-9311-2666

References

[1] Dobson C M 2003 Protein folding and misfolding *Nature* **426** 6968–884
[2] Caughey B and Lansbury P 2003 Protofibrils, pores, fibrils, and neurodegeneration: separating the responsible protein aggregates from the innocent bystanders *Annu. Rev. Neurosci.* **26** 267–98
[3] Hoshino M 2017 Fibril formation from the amyloid-β peptide is governed by a dynamic equilibrium involving association and dissociation of the monomer *Biophys. Rev.* **9** 9–16
[4] Huang X *et al* 2018 Fast, long-term, super-resolution imaging with Hessian structured illumination microscopy *Nat. Biotechnol.* **36** 451
[5] Bastiaens P H and Anthony S 1999 Fluorescence lifetime imaging microscopy: spatial resolution of biochemical processes in the cell *Trends Cell Biol.* **9** 48–52
[6] Kaminski Schierle G S *et al* 2011 A FRET sensor for non-invasive imaging of amyloid formation in vivo *ChemPhysChem* **12** 673–80
[7] Chen W, Young L J, Lu M, Zaccone A, Ströhl F, Yu N, Kaminski Schierle G S and Kaminski C F 2016 Fluorescence self-quenching from reporter dyes informs on the structural properties of amyloid clusters formed *in vitro* and in cells *Nano Lett.* **17** 143–9
[8] Gustafsson M G 2000 Surpassing the lateral resolution limit by a factor of two using structured illumination microscopy *J. Microsc.* 82–7
[9] Hell S W and Wichmann J 1994 Breaking the diffraction resolution limit by stimulated emission: stimulated-emission-depletion fluorescence microscopy *Opt. Lett.* **19** 780–2
[10] Rust M J, Bates M and Zhuang X 2006 Sub-diffraction-limit imaging by stochastic optical reconstruction microscopy (STORM) *Nat. Methods* **3** 793
[11] Betzig E, Patterson G H, Sougrat R, Lindwasser O W, Olenych S, Bonifacino J S, Davidson M W, Lippincott-Schwartz J and Hess H F 2006 Imaging intracellular fluorescent proteins at nanometer resolution *Science* **15 313** 1642–5
[12] Zhu L, Zhang W, Elnatan D and Huang B 2012 Faster STORM using compressed sensing *Nat. Methods* **9** 721
[13] Burnette D T, Sengupta P, Dai Y, Lippincott-Schwartz J and Kachar B 2011 Bleaching/blinking assisted localization microscopy for superresolution imaging using standard fluorescent molecules *Proc. Natl Acad. Sci.* **108** 21081–6
[14] Dertinger T, Colyer R, Iyer G, Weiss S and Enderlein J 2009 Fast, background-free, 3D super-resolution optical fluctuation imaging (SOFI) *Proc. Natl Acad. Sci.* **106** 22287–92
[15] Gustafsson N, Culley S, Ashdown G, Owen D M, Pereira P M and Henriques R 2016 Fast live-cell conventional fluorophore nanoscopy with ImageJ through super-resolution radial fluctuations *Nat. Commun.* **7** 12471
[16] Huang F, Schwartz S L, Byars J M and Lidke K A 2011 Simultaneous multiple-emitter fitting for single molecule super-resolution imaging *Biomed. Opt. Express* **2** 1377–93
[17] Holden S J, Uphoff S and Kapanidis A N 2011 DAOSTORM: an algorithm for high-density super-resolution microscopy *Nat. Methods* **8** 279
[18] Marsh R J, Pfisterer K, Bennett P, Hirvonen L M, Gautel M, Jones G E and Cox S 2018 Artifact-free high-density localization microscopy analysis *Nat. Methods* **15** 689
[19] Cox S, Rosten E, Monypenny J, Jovanovic-Talisman T, Burnette D T, Lippincott-Schwartz J, Jones G E and Heintzmann R 2012 Bayesian localization microscopy reveals nanoscale podosome dynamics *Nat. Methods* **9** 195
[20] Haass C, Kaether C, Thinakaran G and Sisodia S 2012 Trafficking and proteolytic processing of APP *Cold Spring Harbor Perspect. Med.* **2** a006270
[21] Marsh J and Alifragis P 2018 Synaptic dysfunction in Alzheimer's disease: the effects of amyloid beta on synaptic vesicle dynamics as a novel target for therapeutic intervention *Neural Regeneration Res.* **13** 616
[22] Morel E *et al* 2013 Phosphatidylinositol-3-phosphate regulates sorting and processing of amyloid precursor protein through the endosomal system *Nat. Commun.* **2** 2250
[23] Xu H, Greengard P and Gandy S 1995 Regulated formation of golgi secretory vesicles containing alzheimer beta-amyloid precursor protein *J. Biol. Chem.* **270** 23243–5
[24] Kinoshita A 2003 Demonstration by FRET of BACE interaction with the amyloid precursor protein at the cell surface and in early endosomes *J. Cell Sci.* **116** 3339–46
[25] Mizuguchi M, Ikeda K and Kim S U 1992 Differential distribution of cellular forms of beta-amyloid precursor protein in murine glial cell cultures *Brain Res.* **584** 219–25
[26] Jin S, Kedia N, Illes-Toth E, Haralampiev I, Prisner S, Herrmann A and Bieschke J 2016 Amyloid-β (1–42) aggregation initiates its cellular uptake and cytotoxicity *J. Biol. Chem.* **291** 19590–606
[27] Esbjörner E K, Chan F, Rees E, Erdelyi M, Luheshi L M, Bertoncini C W, Kaminski C F, Dobson C M and Schierle G S 2004 Direct observations of amyloid β self-assembly in live cells provide insights into differences in the kinetics of $A\beta$(1–40) and $A\beta$(1–42) aggregation *Chem. Biol.* **21** 732–42
[28] Selkoe D J and Hardy J 2016 The amyloid hypothesis of Alzheimer's disease at 25 years *EMBO Mol. Med.* **8** 595–608
[29] Tiiman A, Krishtal J, Palumaa P and Tõugu V 2015 *In vitro* fibrillization of Alzheimer's amyloid-β peptide (1–42) *AIP Adv.* **5** 092401
[30] Feig M, Yu I, Wang P H, Nawrocki G and Sugita Y 2017 Crowding in cellular environments at an atomistic level from computer simulations *J. Phys. Chem.* B **121** 8009–25
[31] Ami D, Natalello A, Lotti M and Doglia S M 2013 Why and how protein aggregation has to be studied *in vivo Microbial Cell Factories* **12** 17
[32] Nilsberth C *et al* 2001 The 'Arctic' APP mutation (E693G) causes Alzheimer's disease by enhanced Aβ42 protofibril formation *Nat. Neurosci.* **4** 887–93
[33] Lord A, Kalimo H, Eckman C, Zhang X Q, Lannfelt L and Nilsson L N 2006 The arctic Alzheimer mutation facilitates early intraneuronal Aβ42 aggregation and senile plaque formation in transgenic mice *Neurobiol. Aging* **27** 67–77
[34] Lu M, Williamson N, Mishra A, Michel C H, Kaminski C F, Tunnacliffe A and Schierle G S 2019 Structural progression of amyloid-β Arctic mutant aggregation in cells revealed by multiparametric imaging *J. Biol. Chem.* **294** 1478–87
[35] Yu Y, Jans D C, Winblad B, Tjernberg L O and Schedin-Weiss S 2018 Neuronal Aβ42 is enriched in small vesicles at the presynaptic side of synapses *Life Sci. Alliance* **1** e201800028
[36] Kubánková M, López-Duarte I, Bull J A, Vadukul D M, Serpell L C, de Saint Victor M, Stride E and Kuimova M K 2017 Probing supramolecular protein assembly using covalently attached fluorescent molecular rotors *Biomaterials* **139** 195–201
[37] Mlodzianoski M J, Cheng-Hathaway P J, Bemiller S M, McCray T J, Liu S, Miller D A, Lamb B T, Landreth G E and Huang F 2018 Active PSF shaping and adaptive optics enable volumetric localization microscopy through brain sections *Nat. Methods* **15** 583
[38] Wakabayashi K, Tanji K, Mori F and Takahashi H 2007 The Lewy body in Parkinson's disease: Molecules implicated in the formation and degradation of α-synuclein aggregates *Neuropathology* **27** 494–506
[39] Hurtig H I *et al* 2000 Alpha-synuclein cortical Lewy bodies correlate with dementia in Parkinson's disease *Neurology* **54** 1916–21
[40] Conway K A, Lee S J, Rochet J C, Ding T T, Harper J D, Williamson R E and Lansbury P T Jr 2000 Accelerated oligomerization by Parkinson's disease linked α-synuclein mutants *Ann. New York Acad. Sci.* **920** 42–5
[41] Ding T T, Lee S J, Rochet J C and Lansbury P T 2002 Annular α-synuclein protofibrils are produced when spherical

protofibrils are incubated in solution or bound to brain-derived membranes *Biochemistry* **41** 10209–17
[42] Moors T E *et al* 2018 Detailed structural orchestration of Lewy pathology in Parkinson's disease as revealed by 3D multicolor STED microscopy (biorXiv:470476)
[43] Pinotsi D, Michel C H, Buell A K, Laine R F, Mahou P, Dobson C M, Kaminski C F and Schierle G S 2016 Nanoscopic insights into seeding mechanisms and toxicity of α-synuclein species in neurons *Proc. Natl Acad. Sci.* **113** 3815–9
[44] Descloux A *et al* 2018 Combined multi-plane phase retrieval and super-resolution optical fluctuation imaging for 4D cell microscopy *Nat. Photon.* **12** 165
[45] Shahmoradian S H *et al* 2019 Lewy pathology in Parkinson's disease consists of crowded organelles and lipid membranes *Nat. Neurosci.* **22** 1099
[46] Lautenschläger J *et al* 2018 C-terminal calcium binding of α-synuclein modulates synaptic vesicle interaction *Nat. Commun.* **9** 712
[47] Lieberman A P, Shakkottai V G and Albin R L 2019 Polyglutamine repeats in neurodegenerative diseases *Annu. Rev. Pathol.* **14** 1–27
[48] Lu M, Boschetti C and Tunnacliffe A 2015 Long term aggresome accumulation leads to DNA damage, p53-dependent cell cycle arrest, and steric interference in mitosis *J. Biol. Chem.* **290** 27986–8000
[49] Bonfanti S, Lionetti M C, Fumagalli M R, Chirasani V R, Tiana G, Dokholyan N V, Zapperi S and La Porta C A 2019 Molecular mechanisms of heterogeneous oligomerization of huntingtin proteins *Sci. Rep.* **9** 7615
[50] Sakahira H, Breuer P, Hayer-Hartl M K and Hartl F U 2002 Molecular chaperones as modulators of polyglutamine protein aggregation and toxicity *Proc. Natl Acad. Sci.* **99** 16412–8
[51] Sahl S J, Weiss L E, Duim W C, Frydman J and Moerner W E 2012 Cellular inclusion bodies of mutant huntingtin exon 1 obscure small fibrillar aggregate species *Sci. Rep.* **2** 895
[52] Arrasate M, Mitra S, Schweitzer E S, Segal M R and Finkbeiner S 2004 Inclusion body formation reduces levels of mutant huntingtin and the risk of neuronal death *Nature* **431** 805
[53] Johnston J A, Ward C L and Kopito R 1998 Aggresomes: a cellular response to misfolded proteins *J. Cell Biol.* **143** 1883–98
[54] Lu M, Williamson N, Boschetti C, Ellis T, Yoshimi T and Tunnacliffe A 2015 Expression-level dependent perturbation of cell proteostasis and nuclear morphology by aggregation-prone polyglutamine proteins *Biotechnol. Bioeng.* **112** 1883–92
[55] Duim W C, Jiang Y, Shen K, Frydman J and Moerner W E 2014 Super-resolution fluorescence of huntingtin reveals growth of globular species into short fibers and coexistence of distinct aggregates *ACS Chem. Biol.* **9** 2767–78
[56] Bäuerlein F J *et al* 2017 *In situ* architecture and cellular interactions of PolyQ inclusions *Cell* **171** 179–87
[57] Lu M, Banetta L, Young L J, Smith E J, Bates G P, Zaccone A, Schierle G S, Tunnacliffe A and Kaminski C F 2019 Live-cell super-resolution microscopy reveals a primary role for diffusion in polyglutamine-driven aggresome assembly *J. Biol. Chem.* **294** 257–68
[58] Li L, Liu H, Dong P, Li D, Legant W R, Grimm J B, Lavis L D, Betzig E, Tjian R and Liu Z 2016 Real-time imaging of Huntingtin aggregates diverting target search and gene transcription *eLife* **5** e17056
[59] Zhou C, Slaughter B D, Unruh J R, Guo F, Yu Z, Mickey K, Narkar A, Ross R T, McClain M and Li R 2014 Organelle-based aggregation and retention of damaged proteins in asymmetrically dividing cells *Cell* **159** 530–42
[60] Huang C *et al* 2019 Intrinsically aggregation-prone proteins form amyloid-like aggregates and contribute to tissue aging in *Caenorhabditis Elegans eLife* **8** e43059
[61] Zhang K, Zuo W and Zhang L 2018 FFDNet: Toward a fast and flexible solution for CNN-based image denoising *IEEE Trans. Image Process.* **27** 4608–22
[62] Ronneberger O, Fischer P and Brox T 2015 U-net: Convolutional networks for biomedical image segmentation *Medical Image Computing and Computer-Assisted Intervention – MICCAI 2015 Proc., Part III* ed N Navab *et al* (Cham: Springer) pp 234–41
[63] Nehme E, Weiss L E, Michaeli T and Shechtman Y 2018 Deep-STORM: super-resolution single-molecule microscopy by deep learning *Optica* **5** 458–64
[64] Kraus O Z, Ba J L and Frey B J 2016 Classifying and segmenting microscopy images with deep multiple instance learning *Bioinformatics* **32** i52–9